Use of ATR-FTIR To Study Interdiffusion in Polystyrene and Poly(vinyl methyl ether)

Esmaiel Jabbari and Nicholas A. Peppas*

School of Chemical Engineering, Purdue University, West Lafayette, Indiana 47907

Received July 21, 1992; Revised Manuscript Received January 7, 1993

ABSTRACT: Attenuated total reflection infrared spectroscopy (ATR-FTIR) was used to measure interdiffusion in a polystyrene (PS) and poly(vinyl methyl ether) (PVME) compatible pair below and above the glass transition of PS. A thin PS film was spin cast on an ATR germanium crystal while a PVME film was spin cast on the PS film from water solution. The assembly consisting of the ATR crystal and the two polymer films was heated to the desired interdiffusion temperature, and the ATR-FTIR spectrum was collected in situ. The PVME band at 2820 cm^{-1} and the PS bands at 2850 and 3030 cm^{-1} were used for quantitative analysis of the PS/PVME spectrum. The spectrum was deconvoluted to relate the area under the three peaks to the PS and PVME mole fractions. At 105 °C, corresponding to 5 °C above the glass transition of PS, the interdiffusion coefficient was of the order of 1.1×10^{-12} cm^2/s. Interdiffusion was not dominated by either component, and it was controlled by the rate of swelling of PS by PVME. At 85 °C, corresponding to 15 °C below the glass transition of PS, the interdiffusion was non-Fickian and time dependent. A combination of the Fickian and case-II models was used to fit the data at 85 °C as well as the data at 105 °C. A diffusion coefficient of 4.2×10^{-14} cm^2/s and a relaxation constant of 1.6×10^{-9} cm/s for case-II diffusion was obtained for interdiffusion at 85 °C. The data at 105 and 85 °C had 20% and 70% non-Fickian component, respectively. To our knowledge, this is the first time that case-II diffusion has been observed for diffusion at polymer/polymer interfaces above the entanglement molecular weight for below and above the T_g of the slow-diffusing component.

Introduction

Considerable attention has been devoted in recent years to the development and characterization of miscible polymer blends due to the unique combination of properties that they offer.[1] Diffusion at polymer/polymer interfaces affects the final properties of a polymer bilayer as determined by the thickness of the interface or the concentration profile of the two polymers across the interface.

Voyutskii[2] proposed that after intimate contact is established between two polymer films, adhesion takes place by interdiffusion of polymer segments across the interface and that this interdiffusion depends on the compatibility parameter between the two polymers. Later, de Gennes[3–5] also showed that the extent of interdiffusion in compatible polymer pairs is directly proportional to the Flory interaction parameter.

Diffusion at compatible polymer interfaces can be examined for polymer pairs with similar or dissimilar thermal properties. Interdiffusion in homopolymers, otherwise known as polymer healing, has been studied extensively[6] with techniques such as neutron reflectometry,[7] small-angle neutron scattering,[8] forward recoil spectrometry,[9] Rutherford backscattering spectrometry,[10] secondary ion mass spectrometry,[11] infrared microdensitometry,[12] scanning infrared microscopy,[13,14] and surface-enhanced Raman scattering.[15] Generally, these techniques have excellent spatial resolution of the order of 5–100 Å and require deuterium labeling. Deuteration is a disadvantage as Green and Doyle[16] have shown that it can cause slowing down of interdiffusion in polymer pairs.

A number of techniques have also been developed for measuring interdiffusion in compatible pairs with similar properties. These include the combination of scanning electron microscopy and energy-dispersive spectroscopy,[17] transmission electron microscopy,[18] electron energy loss spectroscopy,[19] X-ray reflectometry,[20] and dynamic light scattering.[21] These techniques are only applicable to polymer pairs that contain a heavy element as a label.

Very limited studies of interdiffusion in dissimilar polymers have been reported. Yang et al.[22] have shown that deuteration can significantly affect the miscibility and phase behavior of polymer blends. For the polystyrene and poly(vinyl methyl ether) pair, the lower critical solution temperature increased from 125 to 165 °C upon deuteration, thus rendering techniques that require deuteration for interdiffusion studies not suitable for miscible polymer pairs. Infrared spectroscopy does not require labeling for diffusion studies as, for example, in the work of High et al.,[23] who have used transmission FTIR to measure mutual diffusion of poly(ethylene-*co*-methacrylic acid), henceforth designated p(E-*co*-MAA), and poly(vinyl methyl ether), henceforth designated PVME. The shift in the absorption band of the p(E-*co*-MAA) carboxyl groups due to interassociation between the acid groups in p(E-*co*-MAA) and the ether groups in PVME was used to monitor the mutual diffusion. Boven et al.[24] used external reflection infrared spectroscopy to qualitatively show evidence for interdiffusion in poly(vinyl chloride) (PVC) and poly(methyl methacrylate) (PMMA) bilayers by following the changes in the absorption bands of PVC and PMMA with diffusion time. Vorenkamp et al.[25] used ATR-FTIR to monitor interdiffusion in a PVC/PMMA polymer pair, but no quantitative analysis of the data was reported. Spectroscopic ellipsometry[26] and optical schlieren[27] techniques also do not require labeling as a probe. These two techniques use the refractive index gradient across the interface as a probe for studying interdiffusion.

This work presents the development and quantitative analysis of polymer/polymer interdiffusion experiments with ATR-FTIR using the compatible polymer pair polystyrene and PVME. ATR-FTIR is distinguished from the techniques mentioned above by several advantages: (i) interdiffusion can be measured in situ, thereby reducing the sampling error; (ii) the diffusion of each component can be monitored independently without deuteration or labeling because both polymers have specific absorption bands in the infrared region, and (iii) diffusion coefficients ranging from 10^{-10} to 10^{-17} cm^2/s can be measured with

0024-9297/93/2226-2175$04.00/0

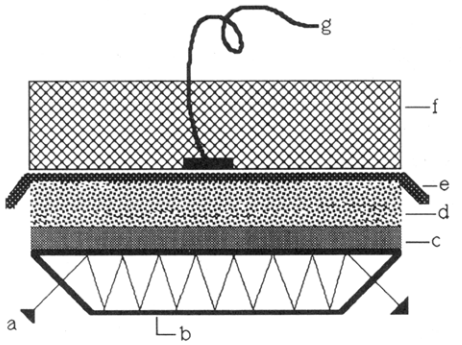

Figure 1. ATR assembly for in situ measurement of polymer/polymer interdiffusion: (a) infrared light beam; (b) ATR crystal; (c) PS layer; (d) PVME layer; (e) aluminum foil; (f) heating unit; (g) thermocouple.

ATR-FTIR spanning temperatures from near or below the glass transition to 100 °C above the glass transition of polymers.

Experimetnal Section

Polystyrene was obtained from Pressure Chemical Co. (Pittsburgh, PA) as a primary standard with a weight-average molecular weight, $\bar{M}_w$, of 105 000 and polydispersity index, PI, of 1.06. PVME was obtained from Scientific Polymer Products (Ontario, NY) as a secondary standard with $\bar{M}_w$ of 99 000 and PI of 2.10. Gel permeation chromatography analysis of the two polymers indicated that no additives were present in the polymers. The GPC was carried out with a GPC system (Model 6000A, Waters Associates, Milford, MA) with tetrahydrofuran as the solvent and μStyragel columns with 10^6-, 10^5-, and 10^3-Å pore sizes and 1 mL/min flow rate.

The PS and PVME samples had T_g of 101 and −27 °C, respectively, measured by differential scanning calorimetry (DSC 2910, E. I. du Pont de Nemours & Co., Wilmington, DE). A thermogravimetric analyzer (Hi-Res TGA 2950, E. I. du Pont de Nemours & Co., Wilmington, DE) was used to study the degradation behavior of PVME and its blends with polystyrene.

A FTIR spectrometer (Nicolet 800, Madison, WI) with the ATR accessory (Connecticut Instruments) was used for the interdiffusion studies in the configuration shown in Figure 1. The ATR crystal was germanium with 5-cm length, 1-cm width, and 2-mm thickness. The polystyrene film was cast on the ATR crystal with a spin coater (Model 1-EC101D-R485, Photo-Resist Spinners, Garland, TX) from a 5% solution in toluene at 250 rpm. The PS film was dried in a controlled atmosphere at 25 °C for at least 24 h, then dried in vacuo at 25 °C for 24 h, and finally heated to 115 °C to remove any residual solvent in the film. The film was annealed at 115 °C for at least 12 h to remove solvent and minimize molecular orientation[28] resulting from the spinning process. The thickness and surface roughness of the PS film were measured using a profilometer (alpha-step 200, Tencor Instruments, Mountain View, CA).

The PVME was cast directly on the PS film from a 10% PVME solution in water using a spin coater at 250 rpm. The high concentration of PVME improved wettability of the solution for PS and gave a continuous layer of PVME on the PS. The PVME film was dried at 25 °C for 24 h and then dried in vacuo at room temperature for 24 h to remove residual water. Since the T_g of PVME is below room temperature, further drying at higher temperatures was not necessary. Sauer and Walsh[26] have used neutron reflection and spectroscopic ellipsometry to study the interface between PS and PVME. They also cast the PVME film directly on the PS from isobutyl alcohol solution. They measured the initial interface thickness with ellipsometry, and in general it was less than 25 nm. Since water is less compatible with PS compared with isobutyl alcohol, the initial interface thickness in our experiments is at most 25 nm. This initial thickness compared with the PS film thickness of 1100 nm would not affect our results significantly.

The thickness of the PVME film was measured by casting a PVME film on a microscope glass slide, with the same dimensions as the germanium crystal, under the same spinning conditions.

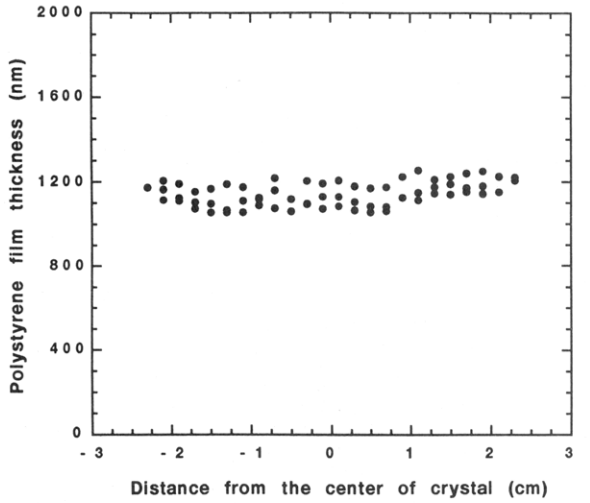

Figure 2. Thickness of the PS film on a germanium crystal. PS with $\bar{M}_w$ of 105 000 and polydispersity index of 1.06 was spin cast at 250 rpm from a 5% toluene solution.

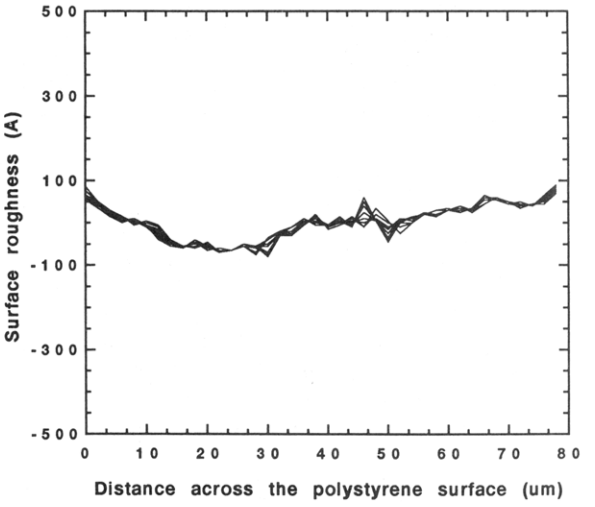

Figure 3. Surface roughness of the PS film on a germanium crystal using profilometry. PS with $\bar{M}_w$ of 105 000 and polydispersity index of 1.06 was spin cast at 250 rpm from a 5% toluene solution.

The film was dried at 25 °C for 24 h and then dried in vacuo at room temperature for 24 h to remove residual water. The glass slide was weighed before and after the PVME film was cast. The thickness of the PVME film was determined from the weight of PVME and the dimensions of the glass slide. The thickness of the PVME film was 6.6 μm, which is the average of four samples. The heating unit was placed on top of the PVME layer with an aluminum foil separating the heating unit from the polymers.

Results

ATR-FTIR was used to measure interdiffusion in a PS/PVME compatible pair below and above the glass transition of PS. Figure 1 shows the schematic diagram of the ATR cell for interdiffusion experiments. The PS film was cast by spin coating from a toluene solution. The thickness and surface roughness of the PS film were measured as a function of distance along the crystal length from the center and are reported in Figures 2 and 3. The PS film thickness was 1.1 μm, and its surface roughness was lower than 200 Å, i.e., about 2% of the total film thickness. The thickness of the PVME film was 6.6 μm. The assembly consisting of the ATR crystal, the two polymer films, and the heating unit was heated to the desired interdiffusion temperature, and the ATR-FTIR spectrum was collected in situ with 128 averaged scans and a resolution of 4 cm^{-1}.

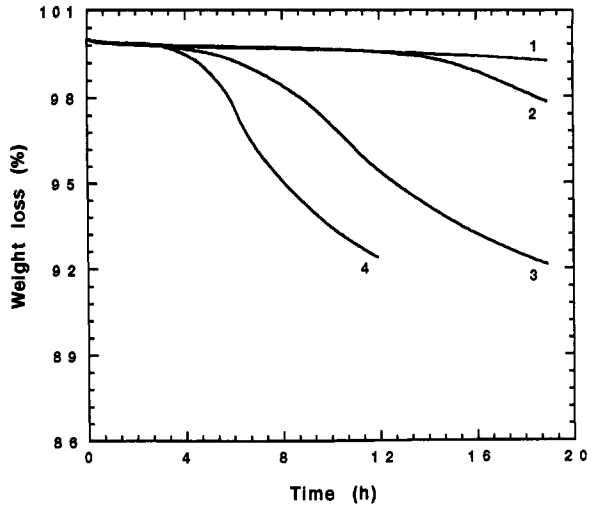

Figure 4. Percent weight loss of PVME as a function of time at 120 (1), 110 (2), 100 (3), and 90 °C, respectively. The $\bar{M}_w$ of PVME and its polydispersity were 99 000 and 2.1, respectively.

Park et al.[29] have studied the oxidation of PVME and its blends with PS. According to their results, the induction period of PVME thermal oxidation was increased by the presence of PS and phase separation occurred shortly before the end of the induction period. They also reported that water vapor and carbon dioxide were evolved during the oxidation of PVME. In our studies, a thermogravimetric analyzer (TGA) was used to monitor the weight loss of PVME as a function of time at temperatures from 90 to 120 °C, as shown in Figure 4. According to Figure 4, there is less than 0.2% weight loss for PVME for 4 h at 120 °C, 5 h at 110 °C, 14 h at 100 °C, and 20 h at 90 °C. Also there was no change in the ATR-FTIR spectra of PS/PVME mixtures during interdiffusion studies.

The phase diagram of a PS/PVME blend changes significantly with molecular weight and molecular weight distribution of the two polymers and with deuteration. Yang et al.[22] have investigated the phase diagram of PS with $\bar{M}_w$ of 100 000 and PI of 1.05 and PVME with $\bar{M}_w$ of 99 000 of PI of 2.13, which are the same molecular weight and polydispersity as for our samples, and they report a LCST of 125 °C. Therefore, the temperature of 105 °C in our experiments is well below the LCST of this blend.

Figure 5 shows the ATR-FTIR spectra of PS and PVME, in the high-frequency region from 2700 to 3200 cm^{-1}. The high-frequency spectra of PS consist of seven absorption bands. The bands with peak locations at 3000, 3030, 3060, 3085, and 3105 cm^{-1} are due to the C–H stretching of benzene ring CH groups on the PS side chain. The bands with peak positions of 2930 and 2850 cm^{-1} are due to the C–H stretching vibration of the CH_2 and CH groups on the main PS chain, respectively. The high-frequency spectra of PVME consist of four absorption bands. The bands with peak positions at 2880, 2930, and 2975 cm^{-1} are due to the C–H stretching vibration of the CH_2 and CH groups on the main PS chain, respectively. The band at 2820 cm^{-1} is the C–H stretching of the CH_3 group of the methoxy side chain, as shown in Figure 5b. Figure 6 shows the ATR-FTIR spectrum of a 50/50 w/w PS/PVME system. The seven absorption bands of PS and the four bands of PVME in the high-frequency region combine to give ten bands with the PS and PVME bands at 2930 cm^{-1} superimposed. No significant change in the peak position or the shape of the bands was observed with temperature or composition.

The PVME band at 2820 cm^{-1} and the PS bands at 2850 and 3030 cm^{-1} were used for quantitative analysis of the

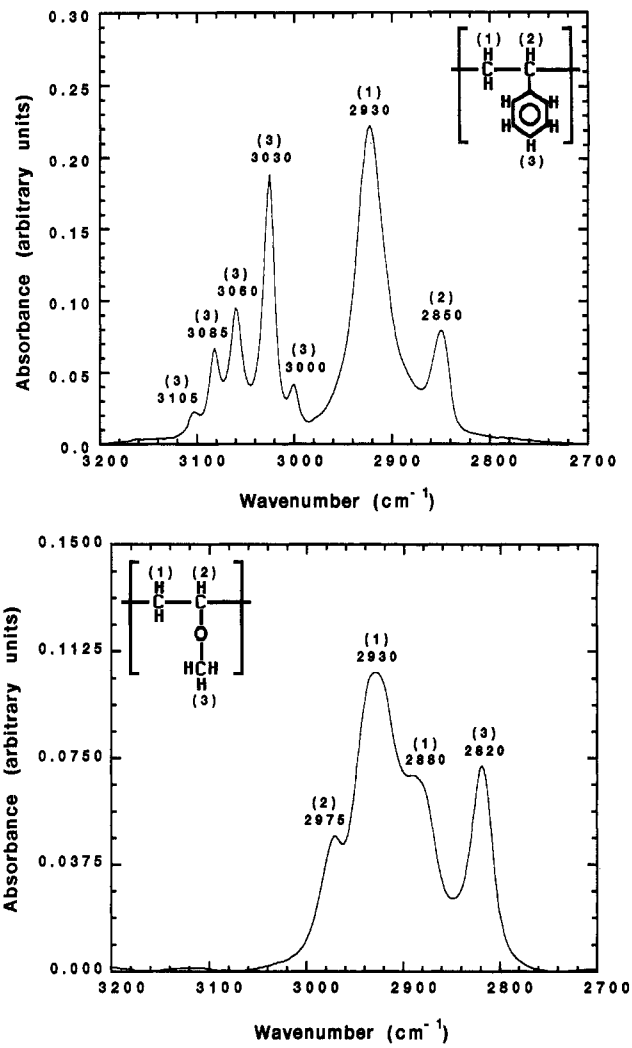

Figure 5. (a, Top) ATR-FTIR spectrum of PS in the high-frequency region. (b, Bottom) ATR-FTIR spectrum of PVME in the high-frequency region.

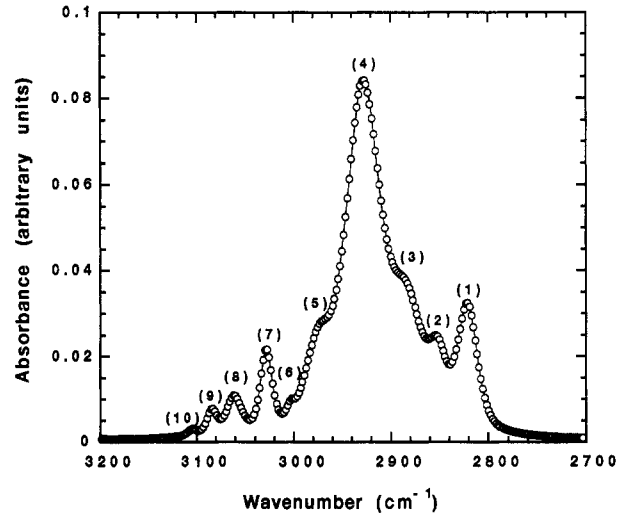

Figure 6. ATR-FTIR spectrum of a 50/50 w/w PS/PVME mixture in the high-frequency region. The open circles and the solid line represent the original and the convoluted spectrum, respectively. The best fit was obtained with a 50% Lorentzian and 50% Gaussian distribution. Peak frequencies (1)–(10) are 2820, 2850, 2880, 2930, 2975, 3000, 3030, 3060, 3085, and 3105 cm^{-1}, respectively.

PS/PVME spectra. The intensity of these three peaks was most sensitive to changes in PS/PVME blend composition. For quantitative analysis, the PS/PVME spectrum was deconvoluted[30] to relate the area under the three

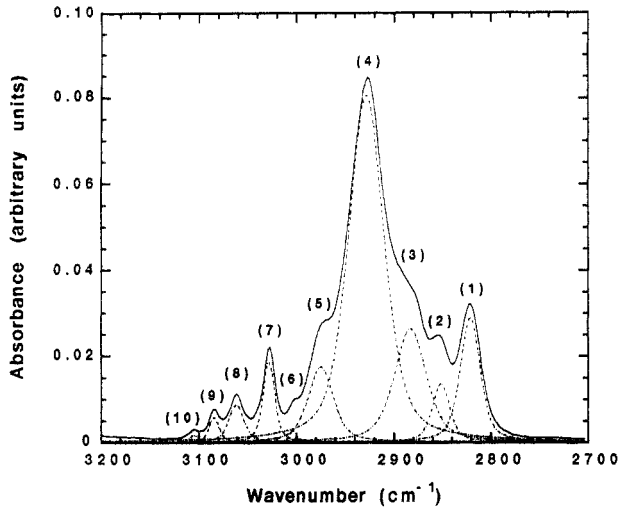

Figure 7. Deconvolution of ATR-FTIR spectrum of a 50/50 w/w PS/PVME blend. The solid line represents the original spectrum, whereas the dotted curves are the deconvoluted peaks using a 50% Lorentzian and 50% Gaussian distribution. Peak frequencies (1)–(10) are 2820, 2850, 2880, 2930, 2975, 3000, 3030, 3060, 3085, and 3105 cm^{-1}, respectively.

peaks to PS and PVME mole fractions. The deconvolution program uses the Levenberg–Marquardt fitting routine to fit the experimental convoluted absorbance data to a set of calculated Gaussian or Lorentzian peaks. The input to the deconvolution program provides the initial guesses for frequency, absorbance, and line width for each peak in the spectrum. The routine ZXSSQ, which is an IMSL (International Math and Statistics Library) routine, is used to minimize the difference between M data points y_i (i = 1,M) and a set g_i calculated from N unknown variables x_j (j = 1,N), as given by the following equation:

$$f_i(x) = y_i - g_i(x) \tag{1}$$

Here, $f_i(x)$ are the residuals, y_i are the data points consisting of absorbance versus frequency, and $g_i(x)$ represent the reconstructed absorbance spectrum from a set of Gaussian or Lorentzian peaks with unknown variables x_j (j = 1,N). The uptake to the unknown variable x is determined by the following equation, which is the focus of the Levenberg–Marquardt algorithm:

$$x^{n+1} = x^n - [\alpha^n \mathbf{D}_n + \mathbf{J}_n{}^T \mathbf{J}_n]^{-1} \mathbf{J}_n{}^T f(x^n) \tag{2}$$

Here, x^{n+1} and x^n are the update and the previous values of the unknown variables x_j (j = 1,n), respectively, $\mathbf{J}_n$ is the forward difference Jacobian matrix evaluated at x^n, $\mathbf{J}_n{}^T$ is the transpose of $\mathbf{J}_n$, $\mathbf{D}_n$ is a diagonal matrix equal to the diagonal $\mathbf{J}_n{}^T\mathbf{J}_n$, and α_n is the Marquardt parameter.

If the Marquardt parameter α is zero, the update is a conventional Newtonian step. As α is increased, it enhances the steepest descent portion of the step (i.e., the diagonal matrix $\mathbf{D}_n$). The routine converges if the residual sum of the squares is less than a prescribed tolerance. Figures 6 and 7 show the comparison of the actual and deconvoluted ATR-FTIR spectrum for a 50/50 w/w PS/PVME mixture. The best fit was obtained with a 50% Lorentzian and 50% Gaussian peaks.

To relate the molar fraction of PVME to the relative absorbance of PVME and PS, a calibration curve was required. Blends of PS and PVME with known composition ranging from 10% to 90% PS by weight were cast on a ZnSe crystal from a 1% solution in toluene at 250 rpm. Toluene is a compatible solvent for PS as well as PVME.[31] The films were dried and annealed above their respective T_g, and their spectra were collected. Figure 8

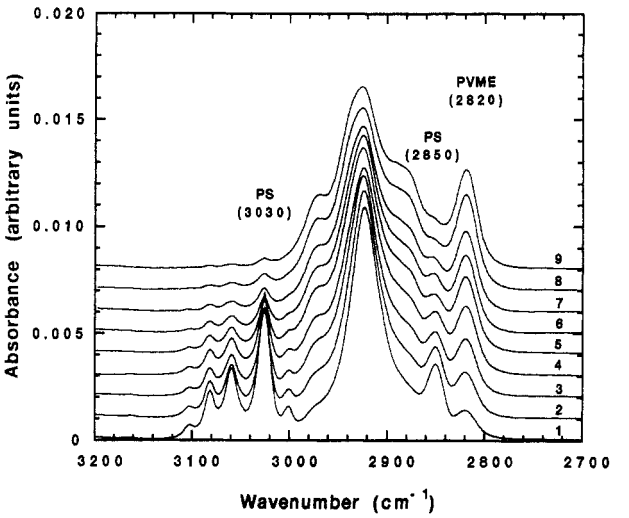

Figure 8. ATR-FTIR spectra of the PS/PVME blends with specified compositions. The PS and PVME $\bar{M}_w$ were 105 000 and 99 000 with polydispersity indices of 1.06 and 2.10, respectively. The films were cast on a ZnSe crystal by spin coating at 250 rpm from a 1% toluene solution. The absorbance scale corresponds to spectrum 1, and the other spectra are shifted by 0.001 absorbance unit. Spectra 1–9 correspond to 90/10, 80/20, 70/30, 60/40, 50/50, 40/60, 30/70, 20/80, and 10/90 w/w PS/PVME blend compositions, respectively.

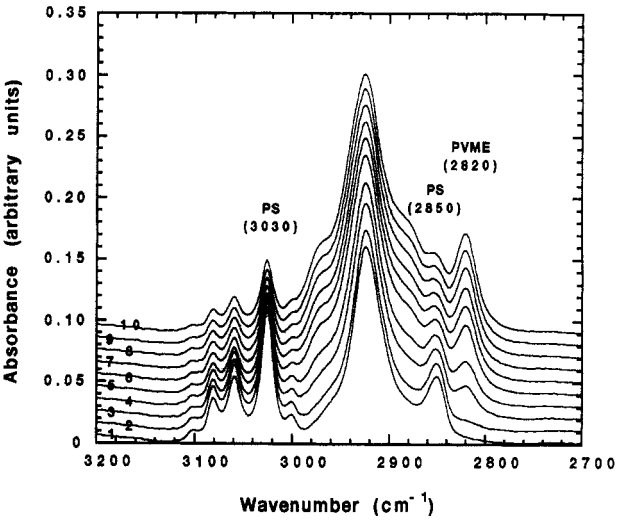

Figure 9. Time evolution of ATR-FTIR spectra for interdiffusion in the PS/PVME pair at 105 °C. The PS and PVME $\bar{M}_w$ were 105 000 and 99 000 with polydispersity indices of 1.06 and 2.10, respectively. The PS film was spin cast on a germanium crystal at 250 rpm from a 5% toluene solution. The PVME film was spin cast on the PS film at 250 rpm from a 10% water solution. The PS and film thicknesses were 1.1 and 6.6 μm, respectively. The absorbance scale corresponds to spectrum 1, and the other spectra are shifted by 0.01 absorbance unit. Spectra 1–10 correspond to 0.0, 0.5, 1.0, 1.5, 2.0, 2.5, 3.0, 4.0, 5.0, and 6.0 h of interdiffusion time, respectively.

shows the ATR-FTIR spectra of nine blends with specified composition. The absorbance scale corresponds to the spectra with 90/10 w/w PS/PVME. The other spectra were shifted by 0.001 absorbance unit each for visual clarity. The areas under the peaks were determined by deconvoluting the original spectrum. The area of the PVME band at 2820 cm^{-1} and the areas of the PS bands at 2850 and 3030 cm^{-1} were used to calculate the relative absorption of PVME and PS.

Figures 9 and 10 show the time evolution of the ATR-FTIR spectra for interdiffusion in the PS/PVME pair at 105 and 85 °C, respectively. The absorbance scale corresponds to the spectrum at zero interdiffusion time.

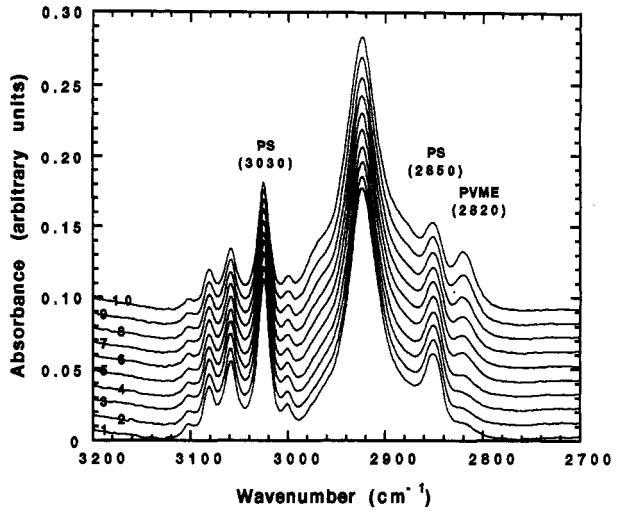

Figure 10. Time evolution of ATR-FTIR spectra for interdiffusion in the PS/PVME pair at 85 °C. The PS and PVME $\bar{M}_w$ were 105 000 and 99 000 with polydispersity indices of 1.06 and 2.10, respectively. The PS film was spin cast on a germanium crystal at 250 rpm from a 5% toluene solution. The PVME film was spin cast on the PS film at 250 rpm from a 10% water solution. The PS and PVME film thicknesses were 1.1 and 6.6 μm, respectively. The absorbance scale corresponds to spectrum 1, and the other spectra are shifted by 0.01 absorbance unit. Spectra 1–10 correspond to 0, 4, 8, 12, 16, 17, 18, 19, 20, and 21 h of interdiffusion time, respectively.

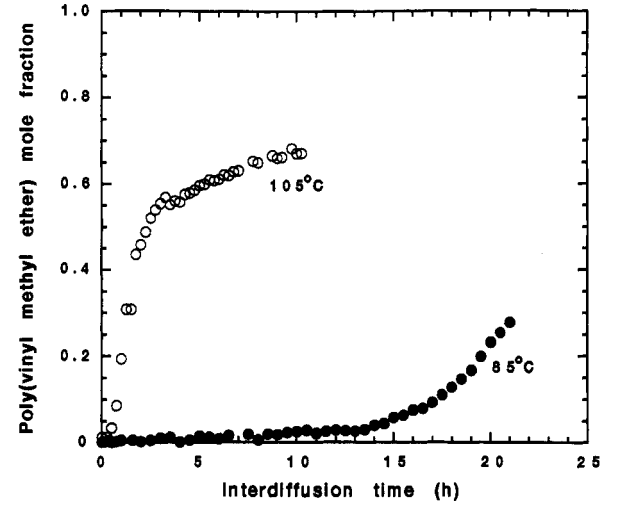

Figure 11. Mole fraction of PVME as a function of time at an interdiffusion temperature of 105 (○) and 85 °C (●). The PS and PVME $\bar{M}_w$ were 105 000 and 99 000 with polydispersity indices of 1.06 and 2.10, respectively. The PS film was spin cast on a germanium crystal at 250 rpm from a 5% toluene solution. The PVME film was spin cast on the PS film at 250 rpm from a 10% water solution. The PS and PVME film thicknesses were 1.1 and 6.6 μm, respectively.

The other spectra were shifted by 0.01 absorbance unit for visual clarity. For the experiment at 105 °C, spectra were collected every 20 min for 10 h, while for the experiment at 85 °C they were collected every 30 min for 22 h. The end-face angle of the ATR crystal and the optical angle of the infrared beam were 45°. As interdiffusion proceeds, the PVME band at 2820 cm^{-1} increases with time and the PS bands at 2850 and 3030 cm^{-1} decrease with time. The spectra were deconvoluted, the relative absorption of PVME as a function of time was calculated, and the molar fraction of PVME was obtained from the calibration curve. Figure 11 shows the comparison of interdiffusion in a PS/PVME pair at 85 and 105 °C as a function of interdiffusion time. At 105 °C, corresponding to 5 °C above the T_g of PS, interdiffusion is fast and reaches

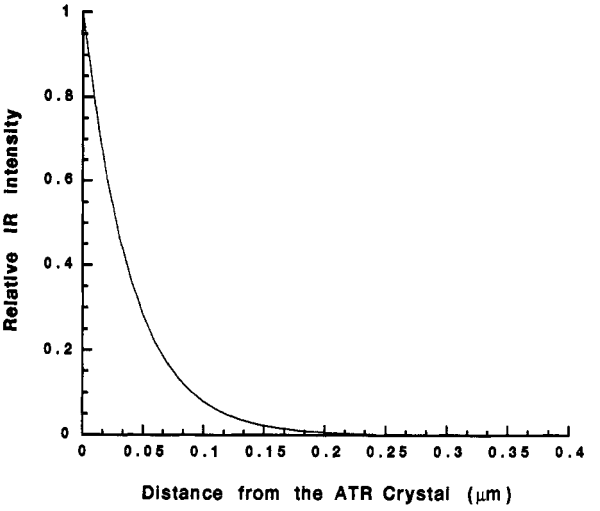

Figure 12. Relative IR intensity in the high-frequency region for the PS layer calculated with eqs 3 and 4. The crystal was germanium with an end-face angle of 45°, and the optical angle of the beam was 45°. The distances 0 and 0.4 μm are the ATR crystal and the PS layer interface, respectively.

equilibrium in less than 10 h. At 85 °C, corresponding to 15 °C below the T_g of PS, interdiffusion is slow with 15 h of induction time.

Analysis of Results with Fickian and Case-II Diffusion

The relative intensity of the radiation as a function of distance away from the crystal surface is shown in Figure 12 for germanium crystal. The relative intensity is given by the following equation:[32,33]

$$I_{rel} = e^{-z/d_p} \tag{3}$$

Here, I_{rel} is the IR intensity relative to the intensity at the interface, z is the distance from the crystal/polymer interface in the polymer layer, and d_p is the penetration depth of IR radiation in the polymer medium. According to eq 3, the intensity decreases exponentially away from the interface. The penetration depth of IR radiation is given by the following equation:

$$d_p = \frac{\lambda}{4\pi\eta_c[\sin\theta^2 - (\eta_p/\eta_c)^2]^{1/2}} \tag{4}$$

where

$$\theta = \beta - \sin^{-1}\left[\frac{\sin(\beta - \psi)}{\eta_c}\right] \tag{5}$$

Here, λ is the wavelength of infrared radiation, η_c and η_p are the refractive indices of the crystal and polymer, respectively, θ is the incidence angle of the beam, β is the end-face angle, and ψ is the optical angle of the beam.

Figure 13 shows the variation of penetration depth with frequency for the refractive index of PS and PVME when using a germanium crystal with end-face and optical angles of 45°. Figure 13 indicates that the penetration depth is a strong function of frequency. For quantitative analysis of the experimental data it is important for the penetration depth to be independent of frequency and changes in refractive index as interdiffusion proceeds. This implies that the higher frequency region of the IR spectrum would be more useful for quantitative analysis. Lu et al.[34] have studied the effect of composition, solvent, and thermal history on position and shape of the PS/PVME FTIR spectrum. In the infrared spectrum of PVME a strong doublet at 1085 and 1107 cm^{-1} with a shoulder at 1132

cm^{-1} showed the greatest change in relative intensity with temperature. Their results also showed that specific absorptions in PSA at 700 cm^{-1} and in PVME at 1100 cm^{-1} are most sensitive to compatibility. They observed no significant change in position or shape of the absorption bands in the higher frequency region of the spectrum as a function of temperature and compatibility.

Fickian Model. The interdiffusion system consists of a PS layer with thickness δ_1 and a PVME layer with thickness δ_2 on an ATR crystal, as shown in Figure 1. The interdiffusion direction is along the z-axis, which is perpendicular to the PS/PVME interface with the origin at the crystal/PS interface. The differential equation describing the diffusion of the PS component across the interface as a function of distance and time with a constant diffusion coefficient is given by the following equation:

$$\frac{\partial c_{PS}}{\partial t} = \frac{\partial}{\partial z}\left(D_{ic}\frac{\partial c_{PS}}{\partial z}\right) \tag{6}$$

Here, c_{PS} is the molar concentration of PS, D_{ic} is the interdiffusion coefficient, z is the distance across the interface, and t is the interdiffusion time. The initial and boundary conditions for solving the above diffusion equation are given by the following equations:

$$c_{PS} = c_0 \qquad 0 \le z \le \delta_1, \qquad t = 0 \tag{7}$$

$$c_{PS} = 0 \qquad \delta_1 < z \le \delta_1 + \delta_2, \qquad t = 0 \tag{8}$$

$$\partial c_{PS}/\partial z = 0 \qquad z = 0, \qquad t > 0 \tag{9}$$

$$\partial c_{PS}/\partial z = 0 \qquad z = \delta_1 + \delta_2, \qquad t > 0 \tag{10}$$

Here, c_0 is the initial concentration of PS. Equations 9 and 10 represent no-flux boundary conditions at the PS/crystal and the PVME/heating unit boundaries, respectively. The solution to the diffusion eq 6 with the above boundary is given[35] by the following equation:

$$c_{PS}(z,t) = \frac{c_0}{2}\sum_{n=-\infty}^{n=+\infty}\left[\operatorname{erf}\left(\frac{\delta_1 + 2n(\delta_1+\delta_2) - z}{2(D_{ic}t)^{1/2}}\right) + \operatorname{erf}\left(\frac{\delta_1 + 2n(\delta_1+\delta_2) + z}{2(D_{ic}t)^{1/2}}\right)\right] \tag{11}$$

The concentration of PVME, c_{PV}, is given by

$$c_{PV}(z,t) = c_0 - c_{PS}(z,t) \tag{12}$$

ATR-FTIR Cumulative Concentration versus Time. The exponential decrease of IR intensity within the penetration depth has to be considered in order to compare experimental results with the model predictions. For an interdiffusion time, t, the concentration of PVME, c_{PV}, at distance z from the crystal surface was multiplied by its corresponding relative intensity, I_{rel}, given by eqs 3 and 4, and it was integrated over the penetration depth of IR radiation inside the polymer layer. This process was repeated for each interdiffusion time to given the cumulative concentration of PVME inside the penetration depth versus time as given by the following equation:

$$Q_{PV}(t) = \frac{\int_0^\infty c_{PV}(z,t)\, I_{rel}(z)\, dz}{\int_0^\infty I_{rel}(z)\, dz} \tag{13}$$

Figure 14 shows the cumulative concentration of PVME for diffusion coefficients of the order of 10^{-12} and 10^{-14} cm^2/s, PS film thickness of 1.1 μm, PVME film thickness of 6.6 μm, and germanium ATR crystals. The most important feature of Figure 14a is the initial induction time for the PVME to reach the penetration depth; then the PVME molar fraction increases rapidly and reaches the equilibrium mole fraction of the PS/PVME blend. This initial induction time is better illustrated in Figure 14b with a 2 order of magnitude smaller diffusion coefficient compared with that of Figure 14a.

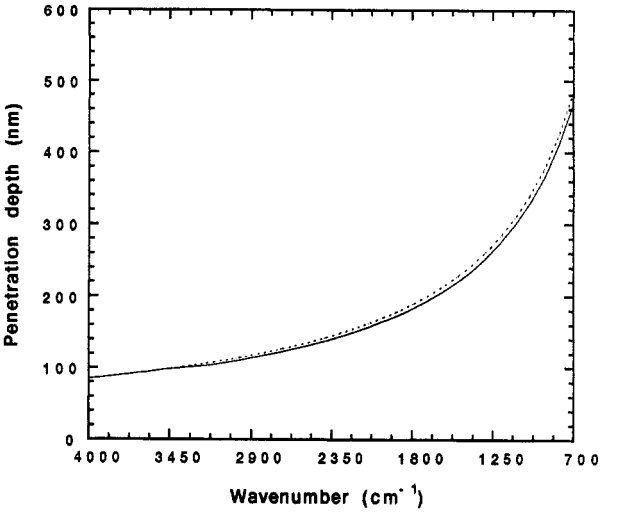

Figure 13. Penetration depth of the IR beam as a function of wavenumber for PS and PVME calculated with eqs 4 and 5. The solid and the dotted lines are for PVME and PS, respectively. The crystal was germanium with an end-face angle of 45°, and the optical angle of the beam was 45°. The refractive indices of the PS and PVME were 1.59 and 1.467, respectively.

Case-II Model. The case-II model corresponds to a diffusion process which depends on the relaxation of the polymer matrix and it is independent of the concentration profile. The faster diffusing component, PVME, diffuses into the slower diffusing component, PS, and the original sharp interface moves into the slower moving component, PS, remaining as a sharp interface. Case-II diffusion is characterized by a relaxation constant, K_{II}, which defines how fast the interface moves into the PS layer. The position of the interface as a function of time is given by the following equation:[36,37]

$$\partial z_{II}/\partial t = -K_{II} \tag{14}$$

Here, z_{II} is the position of the interface as a function of time, t, and K_{II} is the relaxation constant for case-II diffusion. Integrating the above equation subject to the condition that initially the PS/PVME interface is at $z = \delta_1$, the thickness of the PS film, gives the following equation relating the position of the interface to time:

$$z_{II} = \delta_1 - K_{II}t \tag{15}$$

As the PVME diffuses into the PS with a relaxation constant K_{II}, it leaves behind a mixture corresponding to the equilibrium composition of the PS/PVME film. Therefore, the concentration profile is given by the following equations:[37]

$$c_{PV} = c_{PV}^{eq} \qquad z_{II} \le z < \delta_1, \qquad t > 0 \tag{16}$$

$$c_{PV} = 0 \qquad 0 \le z < z_{II}, \qquad t > 0 \tag{17}$$

Here, c_{PV}^{eq} is the equilibrium concentration of PVME and is given by the following equation:

$$c_{PV}^{eq} = \frac{\delta_2\rho_2 M_2^\circ}{\delta_2\rho_2 M_2^\circ + \delta_1\rho_1 M_1^\circ} \tag{18}$$

Here, δ_1 and δ_2 are the thicknesses of the PS and PVME films, respectively, ρ_1 and ρ_2 are the densities of the PS and PVME, respectively, and M_1° and M_2° are the

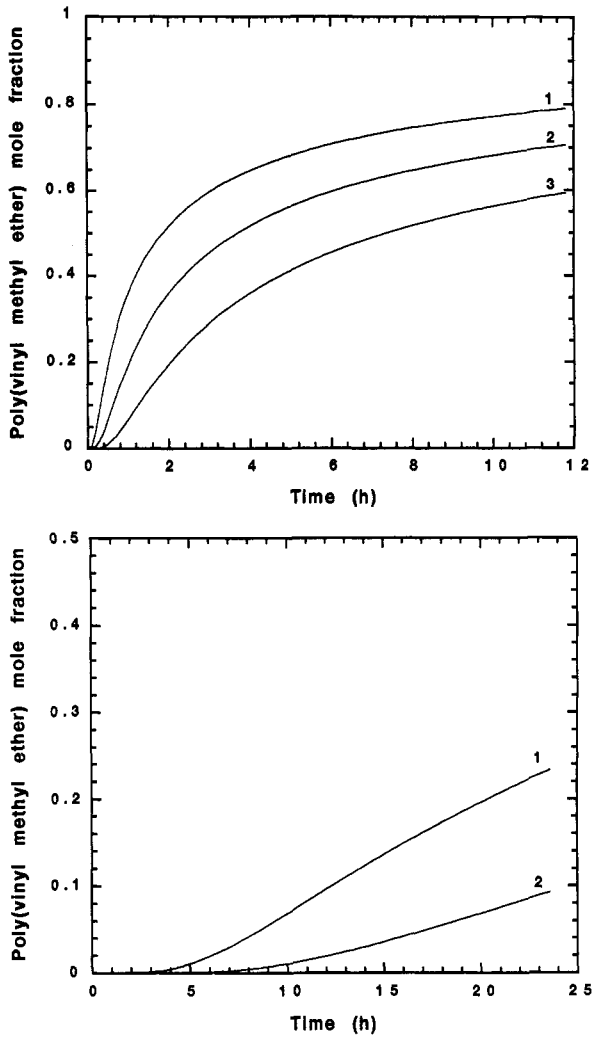

Figure 14. (a, Top) Mole fraction of PVME as a function of interdiffusion time calculated using eqs 11 and 13. The crystal was germanium. The PS and PVME film thicknesses were 1.1 and 6.6 μm, respectively. The penetration depth of the IR beam was 115 nm. Lines 1, 2, and 3 correspond to diffusion coefficients of 0.5×10^{-12}, 1.0×10^{-12}, and 2.0×10^{-12} cm²/s, respectively. (b, Bottom) Mole fraction of PVME as a function of interdiffusion time calculated using eqs 11 and 13. The crystal was germanium. The PS and PVME film thicknesses were 1.1 and 6.6 μm, respectively. The penetration depth of the IR beam was 115 nm. Lines 1 and 2 correspond to diffusion coefficients of 5.0×10^{-14} and 2.5×10^{-14} cm²/s, respectively.

monomer molecular weights of the PS and PVME, respectively. The PVME cumulative concentration inside the penetration depth is determined by substituting for concentration in eq 13 from eqs 16 and 17, which result in the following equation:

$$Q_{PV,II}(t) = \frac{\int_{z_{II}}^{\infty} c_{PV}^{eq} I_{rel}(z)\, dz}{\int_{0}^{\infty} I_{rel}(z)\, dz} \qquad (19)$$

Integrating the above equation and substituting for z_{II} from eq 15 result in the following relation between the PVME cumulative concentration for case-II diffusion and time:

$$Q_{PV,II}(t) = c_{PV}^{eq} \exp\left[\frac{-2(\delta_1 - k_{II}t)}{d_p}\right] \qquad (20)$$

The PVME cumulative concentration may have both Fickian and case-II components. This can be taken into account by using a linear combination of the two cases as given by the following equation:

$$Q_{PV}(t) = (1 - \phi_{II})Q_{PV,F}(t) + \phi_{II}Q_{PV,II}(t) \qquad (21)$$

Here, Q_{PV} is the PVME cumulative concentration inside the penetration depth, $Q_{PV,F}$ and $Q_{PV,II}$ are the Fickian and case-II components of the cumulative concentration, respectively, and ϕ_{II} is the fraction of the case-II component.

Error Analysis. Error analysis was done for eqs 4, 11, and 13 to determine the effect of uncertainty in the values of independent variables on the penetration depth, concentration profile, and the PVME cumulative concentration. The independent variables included refractive index, wavelength, PS and PVME film thickness, and the area of the deconvoluted peaks. The maximum uncertainties expected from the independent variables were 20% for the refractive index, 2% for the wavelength, and 0.1 μm for the PS and PVME film thicknesses. The uncertainties in the areas of the peaks were calculated from the intensity and the line width of each peak which were obtained from their standard deviation based on a 95% confidence level.

The uncertainty in the values of the refractive index and wavelength resulted in less than 1% variation in the penetration depth. The major sources of error for the cumulative concentration of PVME were the uncertainty in the thickness of the PS layer and the area of the deconvoluted peaks. The uncertainty in measuring the PS film thickness and area of the peaks contributed 8% and 10% to the accuracy of the PVME cumulative concentration, respectively, with 15% total error. The uncertainty in the diffusion coefficient obtained by fitting the cumulative concentration of PVME to the Fickian model was 47%. This maximum uncertainty includes the uncertainty in the PS and PVME film thickness, wavelength of the infrared beam, refractive index of the polymers, and the area of the deconvoluted peaks. The error analysis is described in more detail in the Appendix.

Discussion

Figure 15 shows the comparison of the Fickian model prediction based on the solution of eq 13 and the experimentally determined molar fraction of PVME versus time for interdiffusion at 105 °C. The best fit to the experimental data was obtained with a diffusion coefficient of 1.1×10^{-12} cm²/s. The error bars, obtained from the error analysis, are also included for each mole fraction of PVME along with the best fit and the experimental data. The dotted lines above and below the solid line are for diffusion coefficients of 1.2×10^{-12} and 1.0×10^{-12} cm²/s, respectively, to show the sensitivity of the diffusion coefficient to the PVME cumulative concentration. It is important to point out that the best fit using the Fickian model is outside of the error bars for diffusion times of less than 1 h.

Ye et al.[27] have measured the mutual diffusion coefficient for PS/PVME at 112 °C using a modified optical schlieren technique. They report a diffusion coefficient of 1.1×10^{-9} cm²/s for PS and PVME $\bar{M}_w$ of 2950 and 99 000, respectively. After correcting for temperature using the Williams, Landel, and Ferry (WLF) equation, a diffusion coefficient of 7.8×10^{-10} cm²/s at 105 °C is obtained, which is 2 orders of magnitude higher than our experimental value. The PS molecular weight in their experiment was 35 times lower, which was below the entanglement molecular weight. In our experiment, the molecular

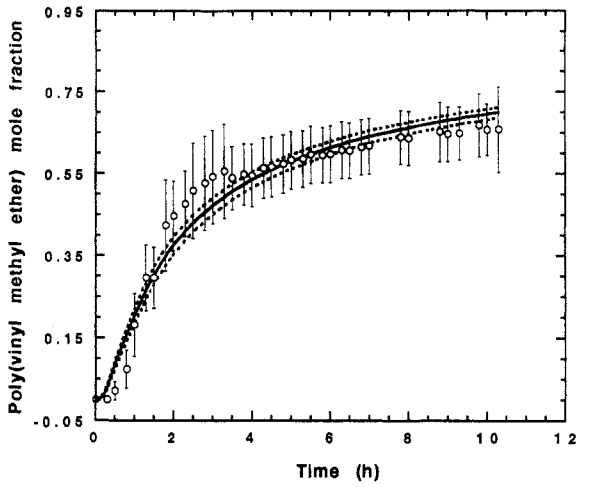

Figure 15. Comparison of the experimental mole fraction of PVME as a function of interdiffusion time and the Fickian model using eqs 11 and 13 at 105 °C. The PS and PVME $\bar{M}_w$ were 105 000 and 99 000 with polydispersity indices of 1.06 and 2.10, respectively. The PS film was spin cast on a germanium crystal at 250 rpm from a 5% toluene solution. The PVME film was spin cast on the PS film at 250 rpm from a 10% water solution. The PS and PVME film thicknesses were 1.1 and 6.6 μm, respectively. The penetration depth of the IR beam was 115 nm. The best fit to the experimental data was obtained with a diffusion coefficient of 1.1×10^{-12} cm²/s.

weights of both PS and PVME were above the entanglement with reptation as the mechanism of diffusion whereas in their experiment, the molecular weight of PS was 6 times lower than the entanglement molecular weight with Rouse as the mechanism of diffusion. Also the T_g of our PS sample was 101 °C whereas T_g for their sample was most likely around 70 °C for PS with a molecular weight of 2950.

Green et al.[38] have measured the diffusion of a PS chain in PS/PVME matrices of different composition with elastic recoil detection. The PS and PVME $\bar{M}_w$ in their studies were 100 000 and 145 000, respectively, which are similar to the molecular weights that we have used. A diffusion coefficient of 1.0×10^{-13} cm²/s was obtained from their experimental results for a 50/50 w/w PS/PVME mixture, after correcting for temperature using the WLF equation. Therefore, our diffusion coefficient is quite reasonable compared with values reported in the literature.

The self-diffusion coefficient of PS and PVME can be calculated from zero-shear viscosity data using the reptation theory.[39] The monomeric self-diffusion coefficient of a polymer chain above the molecular weight from entanglement is related to the monomeric friction coefficient by the following equation:[40]

$$D_i^{m} = \frac{RT}{f_i^{m}} \frac{N_i^{e}}{N_i} \tag{22}$$

Here, f_i^m is the monomeric friction coefficient of component i as if it were a Rouse chain, N_i^e and N_i are the number of repeat units between entanglements and the number of repeat units for chain i, respectively, and R and T are the gas constant and temperature, respectively. Once a mechanism of motion is chosen for the polymer chains, the friction coefficient can be related to the zero-shear viscosity. Graessley[39] has shown that, for the reptation model, the zero-shear viscosity can be related to the friction coefficient by the following equations:

$$\eta_0^{\,i} = \frac{\pi^2}{15} kT \nu_i N_{seg}^{\,i} \tau_d^{\,i} \tag{23}$$

where

$$\tau_d^{\,i} = \frac{1}{kT} \frac{L_i^{\,2}}{\pi^2} \frac{M_i}{M_i^{\circ}} f_i^{m} \tag{24}$$

Here, η_0^i is the zero-shear viscosity of polymer i, τ_d^i is the reptation time of chain i, ν_i is the moles of chain i per unit volume, N_{seg}^i is the number of statistical segments per chain, k is the Boltzmann constant, T is temperature, L_i is the contour length of polymer i, f_i^c is the friction coefficient of the polymer chain, and M_i and M_i° are the molecular weight and monomer molecular weight of polymer i, respectively. Equation 23 relates the zero-shear viscosity of a polymer to its reptation time and, in turn, eq 24 relates the reptation time of a chain to its monomeric friction coefficient. Graessley[41] has also shown that the mesh size of the entangled chains can be related to the mean square end-to-end distance by the following relationships:

$$a_i^{\,2} = \frac{4}{5} \frac{M_i^{e}}{M_i} \langle R_i^{\,2} \rangle_0 \tag{25}$$

where

$$\langle R_i^{\,2} \rangle_0 = L_i a_i \tag{26}$$

Here, $\langle R_i^2 \rangle_0$ is the root mean square end-to-end distance of polymer i, a_i is the mesh size of the entangled chains, and M_i^e is the entanglement molecular weight for polymer i. Substitution of eq 26 in eq 25 results in a relationship between the chain contour length and the mesh size of the entangled chains as given below:

$$L_i = \frac{5}{4} \frac{M_i}{M_i^{e}} a_i \tag{27}$$

Doi et al.[42] have shown that the number of statistical segments, N_{seg}^i, can be related to the mesh size of the entangled chains by the following relation:

$$N_{seg}^{\,i} = \frac{M_i}{M_i^{\circ}} \frac{b_i^{\,2}}{a_i^{\,2}} \tag{28}$$

Here, a_i and b_i are the mesh size of the entangled chains and the statistical segment length, respectively. Rearranging eqs 23–28 results in the following relationship between the zero-shear viscosity and the monomeric friction coefficient:

$$f_i^{m} = \frac{48}{5} \frac{(M_o^{\,i})^2 (M_e^{\,i})^2}{\rho_i b_i^{\,2} M_i^{\,3}} \eta_0^{\,i} \tag{29}$$

The above equation relates the molar monomeric friction coefficient of component i to its corresponding zero-shear viscosity. Shibayama et al.[43] have measured the statistical segment length, b, for PS and PVME blends with different compositions using small-angle neutron scattering. Their results show that the statistical segment length was independent of composition for this mixture and was 7.7 Å. The molecular weights for entanglement for PS and PVME are 18 100[44] and 12 000,[45] respectively. The zero-shear viscosity for PS with $\bar{M}_w$ of 105 000 is 3.16×10^5 P at 170 °C.[46] The zero-shear viscosity for PVME with $\bar{M}_w$ of 99 000 is 1.78×10^4 P at 80.6 °C.[45] The zero-shear viscosity values were corrected for temperature using the WLF equation. Using eqs 22 and 29, the self-diffusion coefficients of PS and PVME are estimated to be 3.06×10^{-19} and 1.44×10^{-10} cm²/s at 105 °C, respectively.

The best fit to the experimental data at 105 °C gives a diffusion coefficient of 1.1×10^{-12} cm^2/s, which is 2 orders of magnitude smaller than the self-diffusion coefficient of PVME and 7 orders of magnitude greater than the self-diffusion coefficient of PS at the same temperature. Although the experimental diffusion coefficient is closer to the PVME self-diffusion coefficient than the PS self-diffusion coefficient, it indicates that the interdiffusion coefficient in the PS/PVME pair above the T_g of the two polymers is not dominated by either the fast or the slow diffusing component.

The fast[47] and slow[48] mode theories for interdiffusion in compatible polymers predict that interdiffusion is dominated by the fast and slow diffusing component, respectively. These theories predict that the concentration profiles are symmetric for interfaces with similar molecular weights and symmetric boundary conditions. Although the fast mode theory predicts swelling of the slow diffusing component by the faster component, this swelling is due to differences in molecular weight and not due to differences in physical properties of the two polymers. There are two major assumptions in these theories which give rise to symmetric concentration profiles.

The first assumption involves the chemical potential of vacancies across the interface. The fast mode theory assumes that the chemical potential gradient of vacancies is zero. This means that the polymer pair is at thermodynamic equilibrium with respect to the surroundings as interdiffusion proceeds.[49] On the other hand, in the slow mode theory, it is assumed that the chemical potential gradient of vacancies is nonzero and dominated by the slow-moving component but the flux of vacancies across the interface is zero. The vacancy chemical potential is related to the relaxation time of the chains as compared to the interdiffusion time.

For PVME to swell the PS matrix, the experimental time should be compared with the relaxation time of PS corresponding to the critical molecular weight for entanglement, M_c. This relaxation time can be estimated using eq 23, which relates the relaxation time of a chain to its zero-shear viscosity. The number of statistical segments per chain, N_{seg}^i, can be estimated if the relaxation time and zero-shear viscosity at one set of conditions are known. The relaxation time of a PS chain with $\bar{M}_w$ of 170 000 at 114.6 °C is 25 min,[50] and the zero-shear viscosity for the same conditions is 6.27×10^{10} P.[46] Substituting for the relaxation time and zero-shear viscosity in eq 23, N_{seg}^i is estimated to be 335 for PS with $\bar{M}_w$ of 170 000. Since the number of statistical segments is inversely proportional to the molecular weight, N_{seg}^i is equal to 71 for PS with M_c of 36 200. Knowing the number of statistical segments, the relaxation time of a PS chain with M_c of 36 200 at 105 °C is 8 s. This relaxation time is an order of magnitude smaller than the experimental time at 105 °C. This indicates that the vacancy chemical potential is not significant above the T_g of PS.

The second assumption involves the concentration dependence of the monomeric friction coefficients or the mobility of the monomer units. The fast mode as well as the slow mode theories assume that the monomeric friction coefficients are independent of composition. Although this is a good assumption for similar polymers with different molecular weights or different polymers with similar properties, this assumption is not valid for polymer pairs with dissimilar properties. We have developed a model[51] based on irreversible thermodynamics for interdiffusion at compatible polymer interfaces with dissimilar properties. This model reduces to the fast mode theory

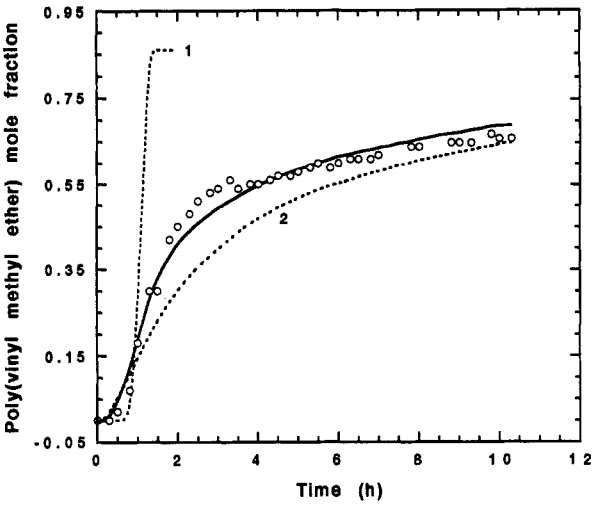

Figure 16. Comparison of the experimental mole fraction of PVME as a function of interdiffusion time and a combination of the Fickian and case-II models using eq 21 at 105 °C. The solid line is the best fit using eq 21, and dotted lines 1 and 2 are the case-II and Fickian components of the best fit, respectively. The PS and PVME $\bar{M}_w$ were 105 000 and 99 000 with polydispersity indices of 1.06 and 2.10, respectively. The PS film was spin cast on a germanium crystal at 250 rpm from a 5% toluene solution. The PVME film was spin cast on the PS film at 250 rpm from a 10% water solution. The PS and PVME film thicknesses were 1.1 and 6.6 μm, respectively. The penetration depth of the IR beam was 115 nm. The best fit to the experimental data was obtained with a diffusion coefficient of 8.8×10^{-13} cm^2/s, the case-II relaxation constant of 3.1×10^{-8} cm/s, and 20% case-II component.

for diffusion at polymer interfaces with similar properties. The results indicate that, for the PS/PVME pair, the concentration profiles are highly unsymmetric with substantial swelling of PS by PVME. This indicates that the assumption of concentration-independent monomeric friction coefficient is not valid for polymer interfaces with dissimilar properties.

For the experimental data at 85 °C, no good fit between the data and the Fickian model was obtained as the interdiffusion coefficient was highly concentration and time dependent. This indicates that interdiffusion below the T_g of PS is highly non-Fickian. The experimental data at 85 °C as well as the data at 105 °C were analyzed using a combination of Fickian and case-II diffusion, given by eq 21. Figures 16 and 17 show the best fit to the PVME cumulative concentration at 105 and 85 °C, respectively. Three parameters were optimized to get the best fit to the experimental data including the Fickian diffusion coefficient, D_{ic}, the case-II relaxation constant, K_{II}, and the case-II fraction, ϕ_{II}.

The best fit to the above parameters is given in Table I. The diffusion coefficient and as the case-II relaxation constant decrease by 1 order of magnitude when the temperature is decreased from 105 to 85°C. More importantly, the cumulative concentration at 105 °C has 20% case-II component whereas the profile at 85 °C has 70% case-II component. This confirms the fact that the concentration profile below the T_g of PS is highly non-Fickian. Also, significant improvement in the correlation coefficient of the best fit was obtained when the data at 105 °C were fitted to a combination of Fickian and case-II models, as shown in Table I.

Figure 18 compares the best fit to the data at 105 °C with the Fickian model and a combination of the Fickian and case-II models. According to Figure 18, the best fit to the Fickian model for times less than 1 h is outside the error bars. However, the best fit using a combination of

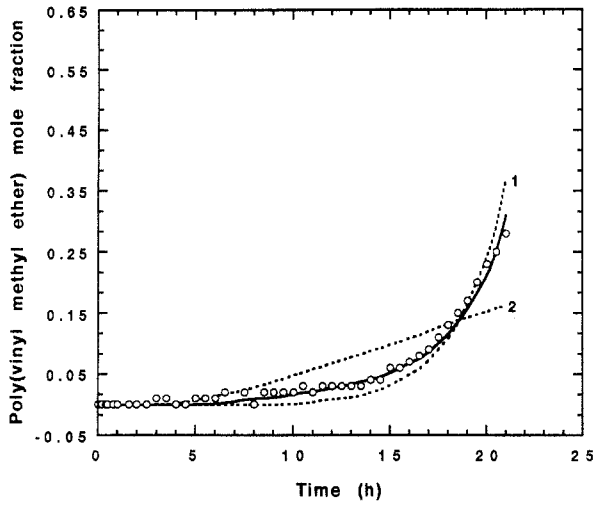

Figure 17. Comparison of the experimental mole fraction of PVME as a function of interdiffusion time and a combination of the Fickian and case-II models using eq 21 at 85 °C. The solid line is the best fit using eq 21, and dotted lines 1 and 2 are the case-II and Fickian components of the best fit, respectively. The PS and PVME $\bar{M}_w$ were 105 000 and 99 000 with polydispersity indices of 1.06 and 2.10, respectively. The PS film was spin cast on a germanium crystal at 250 rpm from a 5% toluene solution. The PVME film was spin cast on the PS film at 250 rpm from a 10% water solution. The PS and PVME film thicknesses were 1.1 and 6.6 μm, respectively. The penetration depth of the IR beam was 115 nm. The best fit to the experimental data was obtained with a diffusion coefficient of 4.2×10^{-14} cm²/s, the case-II relaxation constant of 1.6×10^{-9} cm/s, and 70% case-II component.

Table I
Parameters for the Best Fit of the Experimental Data at 105 and 85 °C to the Fickian and Case-II Models[a]

parameter	T = 105 °C Fickian	T = 105 °C Fickian/case II	T = 85 °C Fickian/case II
D_{ic} (cm²/s)	1.1×10^{-12}	8.8×10^{-13}	4.2×10^{-14}
K_{II} (cm/s)		3.1×10^{-8}	1.6×10^{-9}
ϕ_{II}		0.20	0.70
corr coeff	0.99540	0.99996	0.99624

[a] The parameters D_{ic}, K_{II}, and ϕ_{II} are the Fickian diffusion coefficient, the case-II relaxation constant, and the case-II fraction, respectively. The last row of the table is the correlation coefficient obtained from the best fit.

the Fickian and case-II models is well within the range of the error bars, which indicates there is a non-Fickian component to the concentration profile at 105 °C. To our knowledge, this is the first time that case-II diffusion has been observed for diffusion at polymer/polymer interfaces above the molecular weight for entanglement for above and below the T_g of the slow diffusing component.

Experimental data at 105 and 85 °C clearly indicate that after intimate contact is established between two polymer films, the faster diffusing component swells the slower diffusing component prior to interdiffusion. This swelling has also been observed by others. Sauer et al.[26] used spectroscopic ellipsometry to study the interface between PS and PVME below the T_g of PS. The width of the interface increased from 25 to 50 nm upon annealing at 75 °C for 5 min. Composto et al.[52] used forward recoil spectrometry to study interdiffusion between PS and poly(xylenyl ether) (PXE). PS and PXE have dissimilar properties with T_g's of 100 and 217 °C, respectively. They also observed swelling of PXE by PS when interdiffusion was studied in the range of 7–40 °C below the T_g of PXE. Fernandez et al.[53] used neutron reflectometry to study interdiffusion between poly(methyl methacrylate) (PMMA) and chlorinated polyethylene (CPE). The PMMA and

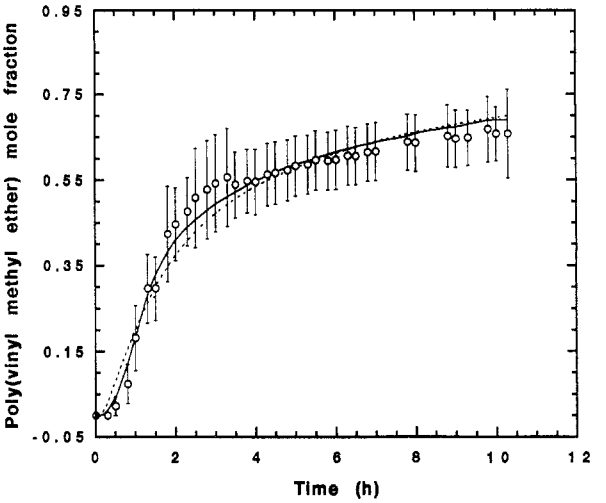

Figure 18. Comparison of the experimental mole fraction of PVME as a function of interdiffusion time with the Fickian model using eqs 11 and 13 and a combination of the Fickian and case-II models using eq 21 at 85 °C. The solid line is the best fit using eq 21, and the dotted line is the best fit using eqs 11 and 13. The PS and PVME $\bar{M}_w$ were 105 000 and 99 000 with polydispersity indices of 1.06 and 2.10, respectively. The PS film was spin cast on a germanium crystal at 250 rpm from a 5% toluene solution. The PVME film was spin cast on the PS film at 250 rpm from a 10% water solution. The PS and PVME film thicknesses were 1.1 and 6.6 μm, respectively. The penetration depth of the IR beam was 115 nm. The best fit using the Fickian model was obtained with a diffusion coefficient of 1.1×10^{-12} cm²/s. The best fit using a combination of the Fickian and case-II models was obtained with a diffusion coefficient of 4.2×10^{-14} cm²/s, the case-II relaxation constant of 1.6×10^{-9} cm/s, and 70% case-II component.

CPE had T_g's of 106 and 116 °C, respectively. For diffusion times smaller than the reptation time of the slower diffusing component (CPE), they observed that the faster diffusing component (PMMA) swelled the slower diffusing component. Stamm et al.[54] used X-ray and neutron reflectometry to study the interface between PS and poly(bromostyrene) (PBrS). The PS and PBrS had T_g's of 100 and 143 °C, respectively. Although this polymer pair is not compatible, they observed the interface thickness increased as much as 1 nm upon annealing at 10–25 °C below the T_g of PBrS. Therefore, the observed swelling of PS below its T_g by PVME is a general phenomenon characteristic of compatible polymer pairs with dissimilar properties.

Conclusions

The ATR-FTIR technique was used to quantitatively measure interdiffusion in a PS/PVME compatible pair. The interdiffusion coefficient at 105 °C was of the order of 1.1×10^{-12} cm²/s, intermediate between the self-diffusion coefficients of PS and PVME. Interdiffusion is not dominated by either component, and it is controlled by the rate of swelling of PS by PVME. The interdiffusion coefficient at 85 °C was non-Fickian and time dependent. A combination of the Fickian and case-II models was used to fit the data at 85 °C as well as the data at 105 °C. A diffusion coefficient of 4.2×10^{-14} cm²/s and a relaxation constant of 1.6×10^{-9} cm/s for case-II diffusion was obtained for interdiffusion at 85 °C. The data at 105 and 85 °C had 20% and 70% non-Fickian component, respectively. The results indicate that in compatible polymer pairs with dissimilar properties, after intimate contact is established between the two polymers, the faster diffusing component swells the slower diffusing component prior to interdiffusion across the interface.

Acknowledgment. This work was presented in preliminary form at the annual meeting of the Adhesion Society in February 1992. It was supported in part by NIH Grant No. GM45027 and by NSF Grant No. CTS-90-07141.

Appendix: Error Analysis

Penetration Depth. The penetration depth is a function of the frequency of the infrared beam and the refractive index of the polymer, as given by eq 4. The uncertainty in the penetration depth is determined using the following equation:

$$\frac{\Delta d_p}{d_p} = \frac{1}{d_p}\frac{\partial d_p}{\partial \lambda}\Delta\lambda + \frac{1}{d_p}\frac{\partial d_p}{\partial \eta_p}\Delta\eta_p \quad (A.1)$$

Δd_p, $\Delta\lambda$, and $\Delta\eta_p$ are the uncertainties in the values of the penetration depth, wavelength, and refractive index of the polymer, respectively. The derivatives of the penetration depth with respect to wavelength and refractive index of the polymer were evaluated using eq 4. The IR bands used for diffusion studies are in the high-frequency region and are separated by 30 cm^{-1}. The maximum uncertainties in the independent variables were 20% for the refractive index, i.e., 0.2, and 2% for wavelength, i.e., 50 cm^{-1}. The above uncertainties resulted in less than 1% variation in the value of the penetration depth.

PVME Cumulative Concentration. The PVME cumulative concentration is related to a number of independent parameters including the thickness of the PS and PVME films, the penetration depth, and the uncertainty in the area of the deconvoluted peaks. The effect of these parameters on the cumulative concentration can be evaluated from the Fickian model using eq 13 and is given by the following equation:

$$\frac{\Delta Q_{PV}}{Q_{PV}} = \frac{1}{Q_{PV}}\frac{\partial Q_{PV}}{\partial A_{PV}^{rel}}\Delta A_{PV}^{rel} + \frac{1}{Q_{PV}}\frac{\partial Q_{PV}}{\partial \delta_1}\Delta\delta_1 + \frac{1}{Q_{PV}}\frac{\partial Q_{PV}}{\partial \delta_2}\Delta\delta_2 + \frac{1}{Q_{PV}}\frac{\partial Q_{PV}}{\partial d_p}\Delta d_p \quad (A.2)$$

where

$$A_{PV}^{rel} = \frac{A_{PV}}{A_{PV} + A_{PS1} + A_{PS2}} \quad (A.3)$$

Here, ΔQ_{PV} is the uncertainty in the value of the cumulative concentration due to uncertainties in the relative absorbance of PVME, ΔA_{PV}^{rel}, the thickness of the PS film, $\Delta\delta_1$, the thickness of the PVME film, $\Delta\delta_2$, and the penetration depth, Δd_p. A_{PV}, A_{PS1}, and A_{PS2} are the areas of the PVME peak at 2820 cm^{-1}, the PS peak at 2850 cm^{-1}, and the PS peak at 3030 cm^{-1}, respectively.

The derivative of Q_{PV} with respect to the relative absorbance of PVME is the slope of the calibration curve. The derivatives of Q_{PV} with respect to δ_1 and δ_2 were evaluated numerically using eqs 11 and 13, and the derivative of Q_{PV} with respect to d_p was evaluated numerically using eqs 3 and 13. For a Gaussian peak, the area of each peak is related to the maximum intensity and line width of the peak by the following equation:

$$A_i = (2\pi)^{1/2} I_i \sigma_i \quad (A.4)$$

Here, I_i and σ_i are the maximum intensity and the line width of peak i, respectively. The uncertainties for the intensity and line width of each peak were obtained from the standard deviation of each variable provided by the deconvolution routine based on a 95% confidence level. The uncertainties for the PS and PVME film thicknesses were 100 nm based on profilometry results. The uncertainty in the values of the penetration depth and the PVME film thickness contributed less than 1% error to the PVME cumulative concentration. The major sources of error were in measuring the thickness of the PS layer and the area of the peaks. The error in measuring the PS film thickness and peak areas contributed 8% and 10% to the uncertainty of the PVME cumulative concentration. This resulted in 18% maximum uncertainty in the value of Q_{PV}.

Diffusion Coefficient. The uncertainty in the diffusion coefficient obtained by fitting the experimental data to the Fickian model is evaluated using the following equation:

$$\frac{\Delta D_{ic}}{D_{ic}} = \frac{1}{D_{ic}}\frac{\partial D_{ic}}{\partial Q_{PV}}\frac{\Delta Q_{PV}}{(n-2)^{1/2}} \quad (A.5)$$

Here, ΔD_{ic} is the uncertainty in the diffusion coefficient due to the uncertainty in the PVME cumulative concentration, ΔQ_{PV}, and n is the number of data points. The derivative of the diffusion coefficient with respect to Q_{PV} was evaluated numerically using eqs 11 and 13. The uncertainty in the diffusion coefficient obtained by fitting the cumulative concentration to the Fickian model was 47%. This maximum uncertain includes the uncertainty in the PS and PVME film thickness, the wavelength of the infrared beam, the refractive index of the polymers, and the area of the deconvoluted peaks.

References and Notes

(1) Klein, J. In *Encyclopedia of Polymer Science and Engineering*; Mark, H., Overberger, C. G., Eds.; Wiley: New York, 1987; Vol. 9, p 205.
(2) Voyutskii, S. S. *J. Adhes.* **1971**, *3*, 69.
(3) de Gennes, P.-G. *J. Chem. Phys.* **1971**, *55*, 572.
(4) de Gennes, P.-G. *J. Chem. Phys.* **1980**, *72*, 4756.
(5) de Gennes, P.-G. *C. R. Acad. Sci., Ser. II* **1981**, *292*, 1505.
(6) Tirrell, M. *Rubber Chem. Technol.* **1984**, *57*, 523.
(7) Karim, A.; Felcher, G. P.; Russell, T. P. *Polym. Prepr. (Am. Chem. Soc., Div. Polym. Chem.)* **1990**, *31* (2), 69.
(8) Roland, C. M.; Bohm, G. G. A. *Macromolecules* **1985**, *18*, 1310.
(9) Mills, P. J.; Green, P. F.; Palmstrom, C. J.; Mayer, J. W.; Kramer, E. J. *Appl. Phys. Lett.* **1984**, *45*, 957.
(10) Green, P. F.; Palmstrom, C. J.; Mayer, J. W.; Kramer, E. J. *Macromolecules* **1985**, *18*, 501.
(11) Whitlow, S. J.; Wool, R. P. *Macromolecules* **1991**, *24*, 5926.
(12) Klein, J.; Briscoe, B. J. *Polymer* **1976**, *17*, 481.
(13) Seggern, J. V.; Klotz, S.; Cantow, H. J. *Macromolecules* **1989**, *22*, 3328.
(14) Jordan, E. J.; Ball, R. C.; Donald, A. M.; Fetters, L. J.; Jones, R. A. L.; Klein, J. *Macromolecules* **1988**, *21*, 235.
(15) Hong, P. P.; Boerio, F. J.; Clarson, S. J.; Smith, S. D. *Macromolecules* **1991**, *24*, 4770.
(16) Green, P. F.; Doyle, B. L. *Macromolecules* **1987**, *20*, 2471.
(17) Gilmore, P. T.; Falabella, R.; Laurence, R. L. *Macromolecules* **1980**, *13*, 33.
(18) Jabbari, E.; Peppas, N. A. *Polym. Bull.* **1991**, *27*, 305.
(19) Klotz, S.; Von Seggern, J.; Kunz, M.; Cantow, H. J. *Polym. Commun.* **1990**, *31*, 333.
(20) Sokolov, J.; Zhao, X.; Rafailovich, M. H.; Bloch, J. M.; Composto, R. J.; Mansfield, T.; Stein, R. S.; Yang, N. L.; Greenbaum, S. G.; Jones, R. A. L.; Kramer, E. J.; Sansone, M. *Polymn. Prepr. (Am. Chem. Soc., Div. Polym. Chem.)* **1990**, *31* (2), 79.
(21) Murschall, U.; Fischer, E. W.; Herkt-Maetzky, C.; Fytas, G. *J. Polym. Sci., Polym. Lett. Ed.* **1986**, *24*, 191.
(22) Yang, H.; Shibayama, M.; Stein, R. S.; Shimizu, N.; Hashimoto, T. *Macromolecules* **1986**, *19*, 1667.
(23) High, M. S.; Painter, P. C.; Coleman, M. M. *Macromolecules* **1992**, *25*, 797.
(24) Boven, G.; Brinkhuis, R. H. G.; Vorenkamp, E. J.; Schouten, A. J. *Macromolecules* **1991**, *24*, 967.

(25) Vorenkamp, E. J.; van Ruiten, J.; Kroesen, F. A.; Meyer, J. G.; Hoekstra, J.; Challa, G. *Polym. Commun.* **1990**, *21*, 325.
(26) Sauer, B. B.; Walsh, D. J. *Macromolecules* **1991**, *24*, 5948.
(27) Ye, M.; Composto, R. J.; Stein, R. S. *Macromolecules* **1990**, *23*, 4830.
(28) Prest, W. M.; Luca, D. J. *J. Appl. Phys.* **1980**, *51* (10), 5170.
(29) Park, H.; Pearce, E. M.; Kwei, T. K. *Macromolecules* **1990**, *23*, 434.
(30) Jabbari, E. J. Ph.D. Thesis, Purdue University, 1993.
(31) Nishi, T.; Kwei, T. K. *Polymer* **1975**, *16*, 285.
(32) Harrick, N. J. *Internal Reflection Spectroscopy*; Wiley: New York, 1967; p 27.
(33) Knutson, K.; Lyman, D. J. In *Biomaterials: Interfacial Phenomena and Applications*; Advances in Chemistry Series 199; American Chemical Society: Washington, DC, 1982; p 197.
(34) Lu, F. J.; Benedetti, E.; Hsu, S. L. *Macromolecules* **1983**, *16*, 1525.
(35) Crank, J. *The Mathematics of Diffusion*; Clarendon Press: Oxford, 1975; p 16.
(36) Berens, A. R.; Hopfenberg, H. B. *Polymer* **1978**, *19*, 489.
(37) Enscore, D. J.; Hopfenberg, H. B.; Stannett, V. T. *Polymer* **1977**, *18*, 793.
(38) Green, P. F.; Adolf, D. B.; Gilliom, L. R. *Macromolecules* **1991**, *24*, 3377.
(39) Graessley, W. W. *J. Polym. Sci., Polym. Phys. Ed.* **1980**, *18*, 27.
(40) Doi, M.; Edwards, S. F. *The Theory of Polymer Dynamics*; Clarendon Press: Oxford, 1986; p 46.
(41) Graessley, W. W. In *Advances in Polymer Science*; Springer-Verlag: Berlin, 1982; Vol. 47, p 67.
(42) Doi, M.; Edwards, S. F. *J. Chem. Soc., Faraday Trans.* **1978**, *74*, 1789.
(43) Shibayama, M.; Yang, H.; Stein, R. S.; Han, C. C. *Macromolecules* **1985**, *18*, 2179.
(44) Ferry, J. D. *Viscoelastic Properties of Polymers*; Wiley: New York, 1980; p 374.
(45) Takahashi, Y.; Suzuki, H.; Nakagawa, Y.; Yamaguchi, M.; Noda, I. *Macromolecules* **1991**, *23*, 1333.
(46) Potter, D. K.; Rudin, A. *Macromolecules* **1991**, *24*, 213.
(47) Kramer, E. J.; Green, P. F.; Palmstrom, C. J. *Polymer* **1984**, *25*, 473.
(48) Brochard, F.; Louffroy, J.; Levinson, P. *Macromolecules* **1983**, *16*, 1638.
(49) Silberberg, A. *Polym. Prepr. (Am. Chem. Soc., Div. Polym. Chem.)* **1991**, *32* (1), 495.
(50) Lee, A.; Wool, R. P. *Macromolecules* **1986**, *19*, 1063.
(51) Jabbari, E.; Peppas, N. A. To be published.
(52) Composto, R. J.; Kramer, E. J.; White, D. M. *Macromolecules* **1988**, *21*, 2580.
(53) Fernandez, M. L.; Higgins, J. S.; Penfold, J.; Shackleton, C. *Polym. Prepr. (Am. Chem. Soc., Div. Polym. Chem.)* **1990**, *31* (2), 71.
(54) Stamm, M.; Reiter, G.; Huttenbach, S.; Foster, M. *Polym. Prepr. (Am. Chem. Soc., Div. Polym. Chem.)* **1990**, *31* (2), 73.